2020

The Role of Vapor Venting and Liquid Feeding on the Dryout Limit of Two-Layer Evaporator Wicks

S. Sukhakar
Purdue University

J. A. Weibel
Purdue University, jaweibel@purdue.edu

F. Zhou
Toyota Research Institute of North America

E. M. Dede
Toyota Research Institute of North America

S V. Garimella
University of Vermont, sureshg@purdue.edu

Sukhakar, S.; Weibel, J. A.; Zhou, F.; Dede, E. M.; and Garimella, S V., "The Role of Vapor Venting and Liquid Feeding on the Dryout Limit of Two-Layer Evaporator Wicks" (2020). *CTRC Research Publications.* Paper 354.
http://dx.doi.org/10.1016/j.ijheatmasstransfer.2019.119063

The Role of Vapor Venting and Liquid Feeding on the Dryout Limit of Two-Layer Evaporator Wicks

Srivathsan Sudhakar[a], Justin A. Weibel[a,1], Feng Zhou[b], Ercan M. Dede[b], Suresh V. Garimella[a2]

[a]School of Mechanical Engineering
Purdue University, 585 Purdue Mall, West Lafayette, IN 47907 USA

[b]Electronics Research Department
Toyota Research Institute of North America, 1555 Woodridge Avenue, MI 48105 USA

Abstract

Vapor chambers developed for high-heat-flux operation require advanced evaporator wick designs that can sustain capillary flow when boiling occurs over the heater region. A two-layer evaporator wick integrates a thin base wick layer that is supplied with liquid from a thick cap layer through an array of vertical feeding posts distributed over the heated area. This design allows boiling to occur within the thin base layer, while separating the incoming liquid feeding and outgoing vapor venting pathways. In our prior work, boiling in two-layer wicks was experimentally demonstrated to provide high-heat-flux dissipation over larger heater areas and at low thermal resistance. The current study experimentally explores the effect of two-layer wick design parameters, specifically the dimensions that alter the area available for liquid feeding and vapor venting, on the thermal performance and dryout limit of the wick, using water as the working fluid. Four different two-layer wick designs are fabricated over a 1 cm^2 evaporator area by sintering 180-212 μm copper particles. Increasing the vapor-venting area from 7% to 16% of the total evaporator area yielded a significant increase in the dryout limit, from 315 W/cm^2 to 405 W/cm^2. Increasing the liquid-feeding area using wider posts increased the dryout limit further. Finally, a parametrically optimized design with fewer but larger posts and vents resulted in better performance compared to a design with denser features. With this two-layer wick design, we demonstrate an extremely high dryout limit of 512 W/cm^2 over the large 1 cm^2 heated area at a thermal resistance of 0.08 K/W.

Keywords

Dryout limit, high-heat-flux dissipation, boiling, two-layer wick, vapor chamber

[1] Corresponding author, E-mail address: jaweibel@purdue.edu
[2] Currently President, University of Vermont

Nomenclature

A	area (m^2)
d	diameter (m)
D	particle diameter (m)
l	length (m)
q	heat flux (W/m^2)
t	thickness (m)

Subscript

base	base wick
bulk	bulk wick
cap	cap layer
evap	evaporator
post	liquid-feeding post
vent	vapor vent

1 Introduction

The miniaturization of electronic devices in computing platforms and power conversion systems has led to tremendously increased heat generation density at both the die and device levels. Thermal management of these high-power-density devices requires advanced cooling architectures where vapor chambers are embedded within the base of the heat sink. Vapor chambers are being increasingly integrated with electronics in this manner owing to their outstanding lateral heat spreading capabilities compared to solid heat spreaders [1].

Phase change within a vapor chamber occurs by evaporation of an internal liquid from a saturated wick at low fluxes; at higher heat fluxes, the process transitions to nucleate boiling. At high heat fluxes, two-phase flow and heat transport in the wick directly above the heated area pose the maximum hydraulic and thermal resistances within the vapor chamber, thereby governing the overall heat spreading performance [2]. The study of boiling in evaporator wicks fed by capillary action has led to a variety of designs for sintered porous [3,4], biporous [5,6,7], and multiscale nanostructured [8,9] wicks to enhance the dryout limit and reduce thermal resistance. However, high-heat-flux dissipation at low thermal resistance with low superheat during capillary-fed boiling has been typically restricted to very small hotspot areas due to the large pressure drop associated with replenishing liquid to the center of the heated area during boiling [10,11]. For larger heater areas, partial dryout has been observed to occur during capillary fed boiling in wicks [3,8], during which a central heated region of the wick does not receive any working fluid. This

causes a local dry spot to form in the center while the surrounding heated area continues to boil, an unfavorable operating regime leading to high surface superheats. Alternatively, thick sintered wicks that provide a large cross section for lateral liquid flow can sustain high heat fluxes over larger areas without drying out, but the pressure drop across the wick thickness associated with vapor outflow from the substrate causes high surface superheats [5].

The need to simultaneously feed liquid while providing pathways for vapor removal through the wick has spurred the development and characterization of hybrid evaporator wicks for use in vapor chambers. Recent developments include evaporator wicks designs having a layer of screen mesh on top of the microchannels [12], lateral converging arteries that feed a thin layer of sintered particles [3], a metal foam layer supplying liquid to thin microposts [13], nano-porous membranes bonded to microchannels [14], or a combination of biporous and monoporous sintered particles [11]. These designs all focus on providing a combination of high permeability to reduce the pressure drop associated with liquid feeding, small pores that provide a high capillary pressure to drive the liquid flow, and vapor removal pathways.

We recently proposed a two-layer evaporator wick concept [15] that was designed to achieve high-heat-flux dissipation over larger heater areas than typically considered in the recent literature. The two-layer wick establishes a flow network for distributed top-down liquid feeding from a cap layer to the heated area through an array of vertical sintered posts, such that boiling can be sustained without drying out in a thin base wick layer. Vents in the cap layer provide preferential pathways for vapor to escape from the wick during intense boiling, thus separating the liquid feeding and vapor removal mechanisms. The dryout limit of the wick was found to be sensitive to the design of the layout of posts and vents. Subsequent fabrication and thermal characterization of the two-layer wick [16] demonstrated that a denser array of posts on the same footprint evaporator area improved the dryout limit of the wick. Distributed liquid feeding by the posts avoids the formation of dry spots in the wick, resulting in low thermal resistance operation across the range of power inputs. In the present work, we performed a targeted parametric study of the role of vapor-venting and liquid-feeding on the dryout limit and thermal performance of the two-layer wick; such a parametric study has not been previously explored. By understanding these effects and appropriately optimizing these parameters of the two-layer wick, we demonstrate high-heat-flux dissipation exceeding 500 W/cm^2 using capillary-fed boiling over large heater areas (1 cm^2).

2 Overview of Fabrication and Testing Procedures

Figure 1 (a) shows a three-dimensional cutaway view of the two-layer evaporator wick structure, with the important features and dimensions labeled. The two-layer wick comprises a base wick layer of thickness, t_{base}, that is supplied by a thick cap layer of thickness, t_{cap}, through an array of vertical liquid feeding posts (diameter, d_{post}). An array of vents of diameter, d_{vent}, are provided in the cap layer, offset from

the posts. The fabrication procedure for the two-layer wick was previously explained in detail in Ref. [16] and is reviewed in brief here. In the first step, a layer of copper particles is sintered flat across a copper substrate. Subtractive laser machining is then used to ablate this layer to form the posts and expose the thin base wick layer over the 1 cm^2 heater area. This first layer is inverted onto a second layer of loose copper particles and sintered, which forms a cap layer that is sintered to the top of the posts. The vapor vents are then laser-machined through the cap layer in positions offset from the posts. To ensure that this process results in connectivity between the two layers of the wick and to confirm alignment between the posts and the vents, SEM images of the wick features were taken between fabrication steps, and a non-destructive micro-CT scan was performed after fabrication [10]. The structures are found to be intact after fabrication and provide the necessary liquid feeding pathway from the cap wick, through the posts, and into the base wick. Figure 1 (b) shows a photograph of the as-fabricated two-layer wick with a 12 × 12 array of liquid feeding posts and a 11 × 11 array of vapor vents (note that the vents are visible in the top-down view).

A capillary-fed boiling test facility, as shown in Figure 2 (a), is used to test the thermal performance of the two-layer wicks. The test facility and procedures are identical to those reported in Ref. [16]. The test facility replicates the working conditions near the evaporator region of a vapor chamber by allowing the working fluid (DI water) to be uniformly drawn into the wick from all directions. In addition, the wick is placed within a chamber that maintains saturation conditions (100 °C, 1 atm). The liquid level in the chamber is higher than the wick level and flooding over the top of the evaporator is prevented by a dam that seals around the wick using a rubber gasket, as shown in Figure 2 (b). Because the capillary pressure of the wick is much larger than the gravitational pressure head, the liquid level above the wick provides negligible assistance to the flow and does not affect the dryout heat flux. The wick is heated over a 1 cm^2 area by soldering the substrate to a copper block with embedded cartridge heaters. A rake of thermocouples embedded in the well-insulated heater block measures the input heat flux and substrate temperature assuming one-dimensional heat flow; thermocouples in the liquid pool and vapor space inside the chamber monitor the temperatures within. A pressure transducer measures the chamber pressure, which is maintained at 1 atm by adjusting the flow rate of coolant (DI water) to the condenser coil within the chamber. A high-speed camera fitted directly above the chamber visualizes and records the boiling process in the wick through a window in the top of the chamber. The videos are obtained at a resolution of 640 × 600 pixels at 2000 frames per second.

Prior to each test, the wick is dipped in a dilute piranha solution, rinsed in DI water, dried thoroughly with compressed nitrogen, and sealed into the chamber. At the start of each test, the working fluid is boiled vigorously in the chamber to purge all dissolved non-condensable gas with a Graham condenser. During testing, the chamber is sealed, and a coolant passes through a copper condenser coil inside the chamber; the coolant enters the coil at a constant temperature controlled by a chiller. To control the saturation pressure

within the chamber, the mass flow rate of the coolant is adjusted using a metering valve. To obtain a boiling curve, the heat input to the sample is turned on and increased in steps; the system is allowed to reach steady state at each step and the thermocouple readings are recorded. Steady state is defined to be reached when the rate of change of temperatures in the heater block is within 0.1 °C/min, over a period of 10 min. The complete data reduction and uncertainty analysis is presented in Ref. [16]. The calibrated thermocouples have a temperature measurement uncertainty of ±0.3 °C with a position uncertainty of ±0.2 mm. The heat flux into the wick is calculated from a linear fit to the thermocouple rake readings in the heater block; the substrate temperature is calculated by extrapolating from the thermocouple reading immediately below the substrate. The uncertainty in the measured heat flux is 5-10%, while the uncertainty in the measured surface superheat was 7-11%, over the range of values reported in this study. The thermal resistance of the wick is defined based on the difference in temperatures of the substrate and the vapor space at a given heat flux.

3 Designs of two-layer wicks

A reduced-order analytical model was previously developed for flow and heat transfer in the two-layer wick [15]. The model predicted that denser post arrays over the evaporator area, which reduce the flow length and thereby pressure drop within the thin boiling wick layer, enhance the dryout limit of the wick. In addition, the vapor flow pressure drop was predicted to be significantly affected by the vapor venting area. At a given post array size, the analysis concluded that the vapor vents must be made as large as possible, up to the physical limit of overlapping with the posts, to minimize the total pressure drop. Prior to the current work, the fabrication and testing of prototype two-layer wick designs evaluated the parametric effects of post array size and sintered copper particle sizes during capillary-fed boiling. The dryout heat flux increased when the post array size was increased from 5 × 5 to 10 × 10 within the same footprint area [16]. Additionally, particle sizes in the range 180 – 212 μm provided the highest dryout limit and lowest thermal resistance [10]. In the current work, geometric design parameters that affect the cross-sectional areas available for vapor venting and liquid feeding are experimentally studied. Different two-layer evaporator wicks were fabricated by independently varying the vent diameter, post diameter, and array pitch. All the designs use sintered copper particles in the size range of 180 – 212 μm. Figure 3 (a) shows a top view of the footprint area that is the same for all evaporator wicks tested in this work. A 30 mm × 30 mm bulk feeding wick (side length, l_{bulk}) supplies a central 10 mm × 10 mm heated evaporator area (side length, l_{evap}). The wick is fabricated on a 1 mm-thick copper substrate of dimensions 38.1 mm × 38.1 mm, per the fabrication procedure outlined in Section 2. The two-layer wick features are fabricated over the 10 mm × 10 mm evaporator area. Figure 3 (b – e) show schematic diagrams of the top views and side views of the different two-layer wick designs (Wicks 1 – 4) for a symmetric quadrant of the evaporator area. The darker filled circles in the top view represent the posts below the cap layer while the open circles represent

the vents in the cap layer. The dimensions of the wick features (array sizes, post diameter, d_{post}, vent diameter, d_{vent}) are tabulated in Table 1. The dimensions that remain constant across the designs are the cap layer thickness, t_{cap} = 800 μm, post thickness, t_{post} = 400 μm, and base layer thickness, t_{base} = 400 μm.

To analyze the effect of vapor venting area on the performance, Wicks 1 and 2 were fabricated with the same 12 × 12 post array and a fixed post diameter, d_{post} = 500 μm. Wick 1 has a sparse 6 × 6 array of vents of diameter d_{vent} = 500 μm, providing a total vapor venting area of ~ 7% of the total cap layer area (A_{vent}/A_{evap}). For Wick 2, additional vapor vents of diameter 500 μm and 300 μm are laser-machined through the cap layer in a different pattern that yields a significantly larger percentage area for venting (A_{vent}/A_{evap} ~ 16%). The post diameters in Wicks 1 and 2 are fixed at 500 μm, which results in only 2.5 sintered particles on average across the cross-section of each post. To increase the feeding area through each post and study its effect on the thermal performance, the post diameter was enlarged to 650 μm in Wick 3, while keeping the same 12 × 12 post array size and venting area compared to Wick 2 (A_{vent}/A_{evap} ~15%). This results in a much denser array of posts than the previous designs, which consequently leads to a complementary reduction in the vapor flow area in the interstices between the posts. Wick 4 is fabricated with the same total venting area (A_{vent}/A_{evap} ~16%) and post diameter (d_{post} = 650 μm) as Wick 3, but the spacing between the posts is increased to allow more vapor flow area between posts, resulting in a 10 × 10 array of posts.

4 Results

The results reported here show boiling curves (heat flux plotted against substrate superheat) in Figure 4 (a) and thermal resistance curves (wick resistance plotted against heat flux) in Figure 4 (b) for each wick tested. Several general trends in these curves are common to all the two-layer wicks. At low fluxes, the space between the posts of the two-layer wick is filled with liquid and active bubbling occurs through the vents. When the heat flux is increased, the liquid recedes and is only present in the wick regions (base layer, cap layer, and the posts), forming a separated pathway for vapor to escape from the wick base layer through these spaces and out of the vents. This mode of operation leads to a reduced thermal resistance at higher heat fluxes because the vapor flow impedance out of the wick is minimized. Due to the distributed liquid feeding across the base layer, the two-layer wicks do not exhibit partial dryout, which would be observed as a gradual increase in thermal resistance leading to complete dryout. Rather, the test is stopped in the present work when a sudden increase in the substrate temperature is triggered by a complete dryout event. The last steady value of the measured heat flux is reported as the dryout heat flux of the wick, and the corresponding thermal resistance is taken as the dryout thermal resistance.

4.1 Effect of vapor-venting area

The area available for vapor venting is observed to significantly affect the dryout limit of the two-layer wick. Comparing the green and blue curves in Figure 4 (a), it is noted that Wick 1 (green curve) dries out at a heat flux of 315 W/cm^2. Increasing the fraction of the cap layer for vapor venting from 7% to 16% in Wick 2 (blue curve) yields an increase in the dryout limit to 405 W/cm^2. We attribute this enhancement to a decrease in the vapor pressure drop through the vents. The thermal resistance curves for Wicks 1 and 2 also exhibit an interesting difference in Figure 4 (b). At low fluxes, the resistance of Wick 2 is greater than the corresponding values of Wick 1. This is because of the greater open volume in the design of Wick 2 compared to Wick 1, such that a larger portion of Wick 2 is flooded with liquid (having lower thermal conductivity than copper) at low fluxes. This causes the measured thermal resistance to be higher in Wick 2 at low fluxes.

Figure 5 shows the top-view visualization images (refer Appendix A for the corresponding videos) taken during the boiling process over the evaporator region for Wicks 1 and 2 at a similar heat flux of ~240 W/cm^2. A critical difference is observed between the vapor venting processes in the two wicks. Wick 1 restricts the pathway for vapor flow out of the wick due to a smaller venting area. Vapor bubbles through the cap layer instead of exiting through the designated vents, which impedes liquid replenishment by the thick cap layer, as shown in the schematic diagram in Figure 5 (a). A transition to this mode of operation causes the measured thermal resistance to increase sharply for heat fluxes greater than 240 W/cm^2 for Wick 1 (as seen in Figure 4). In addition, the maximum heat flux that can be dissipated by Wick 1, which is the lowest of all tested, is limited due to this blockage of liquid supply through the cap layer. In comparison, Wick 2 has a greater vent area for vapor to escape, leading to separated flow pathways where the exiting vapor does not obstruct liquid feeding, as illustrated in the schematic diagram in Figure 5 (b). There is a notable improvement in the maximum dryout heat flux from 315 W/cm^2 for Wick 1 to 405 W/cm^2 for Wick 2. We conclude that the vapor venting area plays a major role in determining the dryout limit, and make the general recommendation that vents should be made as large as possible to minimize the vapor flow pressure drop.

4.2 Effect of post area and post spacing

Dryout can be triggered in the two-layer wick if the posts are not capable of sufficiently feeding the thin base layer. Our prior visualization images of the two-layer wick operation showed that the liquid meniscus recedes into the cap layer and posts as the heat flux increases to high levels [16]. Hence, including more particles across the cross-section of each post can provide a greater area for liquid flow and reduce the chance of the capillary flow path through the post being cut off as the meniscus recedes. All geometric parameters are held constant across Wicks 2 and 3, except that the post diameters are enlarged from 500

μm to 650 μm in Wick 3. From the boiling curves plotted in Figure 4 (a), it is observed that Wick 3 (magenta curve) dries out at a maximum heat flux of 457 W/cm^2, which is a 13% increase over Wick 2 (blue curve). This increase is attributed to the additional liquid feeding area. The thermal resistance curves for these two wicks are very similar; the resistance decreases during the part of the boiling curve at lower heat fluxes and reaches a nearly constant value at higher fluxes. While the dryout limit is enhanced due to the greater cross-sectional area of the posts, this also causes a reduction in the vapor flow area between the spaces of the two-layer wick.

To enhance the dryout limit further, the vapor flow area in the interstices between the posts was increased in Wick 4. This wick was fabricated with the same post diameter (d_{post} = 650 μm) as Wick 3, but the posts were spaced further apart, resulting in a slightly sparser 10 × 10 array of posts as shown in Figure 3 (e). An offset 9 × 9 array of vents of diameter d_{vent} = 500 μm is fabricated to maintain a constant vapor venting area across Wicks 2, 3 and 4. In Figure 4 (a), Wick 4 (red curve) reaches the highest dryout heat flux of ~ 512 (±29) W/cm^2 among the wicks tested. The dryout heat flux is improved from the previous designs due to an effective balance between the liquid feeding cross-sectional area of the posts and the vapor venting areas. The design provides a near-linear increase in the wick superheat with increasing heat fluxes up to complete dryout. The trends in the wick thermal resistance are similar to the previous designs. At lower heat fluxes, the spaces between the posts are flooded with liquid, causing the measured thermal resistance to be higher. With increasing heat flux, the wick provides separated flow pathways for liquid and vapor that causes a reduction in the thermal resistance compared to the values at low heat fluxes. This mechanism is also evident from the visualization videos obtained at different heat fluxes during the boiling process for Wick 4, shown in Appendix A. Wick 4 yields a thermal resistance of 0.08 (±0.01) K/W at dryout, the lowest among the wick designs tested.

5 Conclusions

A two-layer evaporator wick for use in high-heat-flux vapor chambers is designed to effectively supply liquid by capillary action to a thin base layer that is boiling. Liquid is fed to the base layer using an array of posts that are connected to a thick porous cap layer. Vapor vents in the cap layer allow the vapor to easily escape the wick during capillary-fed boiling. In this study, the effects of the vapor-venting and liquid-feeding areas on the dryout heat flux of two-layer wicks were experimentally investigated. Two-layer wicks with different geometric parameters were fabricated and tested. The total vapor venting area was found to significantly influence the dryout limit of the wick. Increasing the fraction of vapor venting area relative to the heated footprint area from 7% to 16% improved the dryout limit of the wick from 315 W/cm^2 to 405 W/cm^2. It was observed from high-speed visualizations that the lower vapor venting area caused vapor to bubble through the cap layer, obstructing the liquid replenishment pathway and reducing the maximum heat

flux. In addition, it was shown that increasing the liquid-feeding area by increasing the cross-sectional area of each post improved the dryout heat flux. Among the tests, a tradeoff was identified: the advantage of increased liquid-feeding area competes with the disadvantage of reducing the area for vapor flow between the posts of the wick. An optimized performance was measured for a 10 × 10 array of 650 μm diameter posts with an offset 9 × 9 array of 500 μm vents. Among all the designs, this wick reached the highest dryout limit of ~ 512 W/cm^2 over a 1 cm^2 heated area at the lowest thermal resistance of 0.08 K/W.

The results of this study offer general guidance on the design of two-layer evaporator wicks. Optimal designs should feature the maximum possible vapor venting area in the cap layer within the limits achievable by the fabrication process. In addition, the post and vent arrays must be designed with care to achieve a balance between the liquid feeding and vapor venting areas. Further performance improvements may be possible by exploring alternative wick compositions, aside from monoporous sintered copper particles, to be used as the thin base layer for increasing the dryout limit during capillary-fed boiling.

Acknowledgements

This material is based upon work supported by Toyota Motor Engineering and Manufacturing North America, Inc. under an Advanced Research Collaboration between Purdue University and the Toyota Research Institute of North America.

Appendix A

The supplementary high-speed videos associated with the article can be found online.

List of Tables

List of Figures

Table 1. Key dimensions and geometric parameters of the two-layer wick samples tested. The wicks are fabricated using 180 – 212 μm size particles; the dimensions that remain constant across the designs are t_{cap} = 800 μm, t_{post} = 400 μm, and t_{base} = 400 μm.

Sample ID	**Post Array**	**Vent array**	**Post diameter d_{post} (μm)**	**Vent diameter d_{vent} (μm)**	**Fraction of vent area (A_{vent}/A_{evap})**	**Fraction of post area (A_{post}/A_{evap})**	**Dryout heat flux (W/cm^2)**
Wick 1	12 × 12	6 × 6	500	500	0.07	0.28	315
Wick 2	12 × 12	11 × 11	500	500/300	0.16	0.28	405
Wick 3	12 × 12	11 × 11	650	400	0.15	0.48	457
Wick 4	10 × 10	9 × 9	650	500	0.16	0.33	512

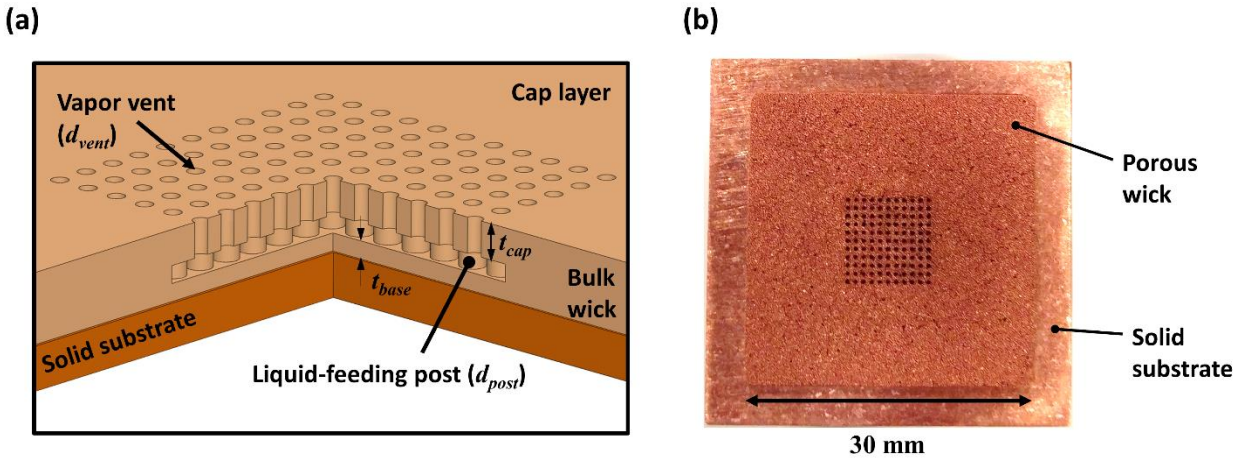

Figure 1. (a) Schematic diagram (to scale) showing a 3D perspective view of the two-layer wick region (12 × 12 posts, 11 × 11 vents) with a quarter cut out along symmetry planes to reveal the internal features and key dimensions. (b) Photograph of the fabricated two-layer evaporator wick on a copper substrate.

(note for editor: 1.5 column wide)

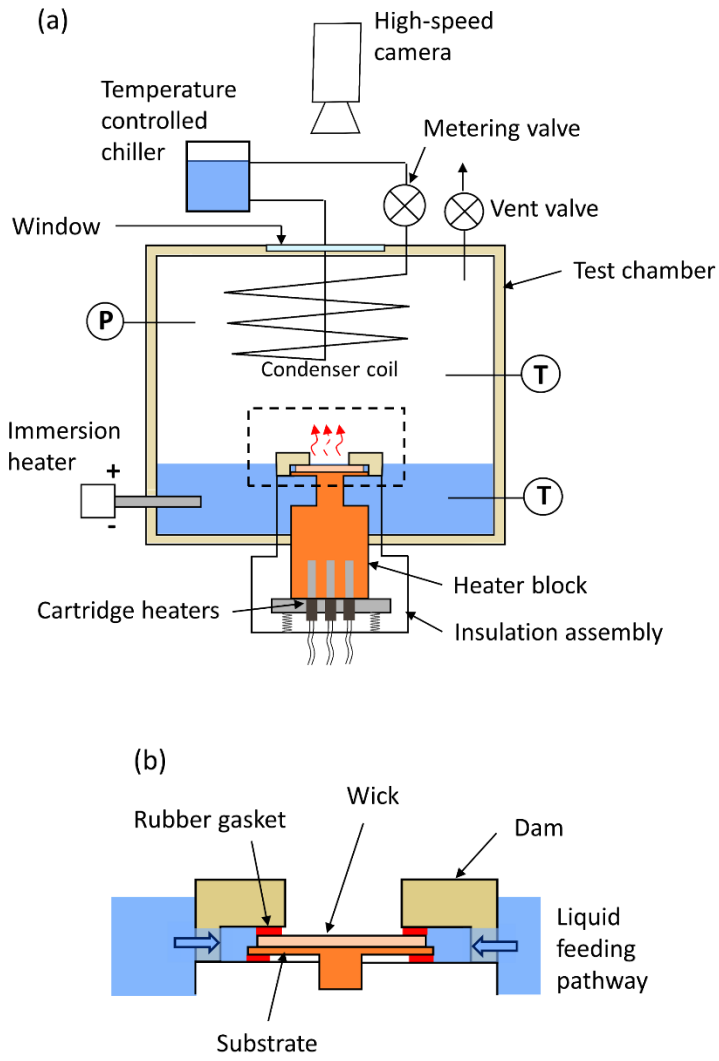

Figure 2. (a) Schematic diagram of the capillary-fed boiling test facility that consists of a saturated test chamber and a heater block assembly, with key components labeled. (b) A close-up view near the wick showing the liquid flow pathway into the wick from the sides; the dam prevents flooding over the top of the wick.

(note for editor: 1 column wide)

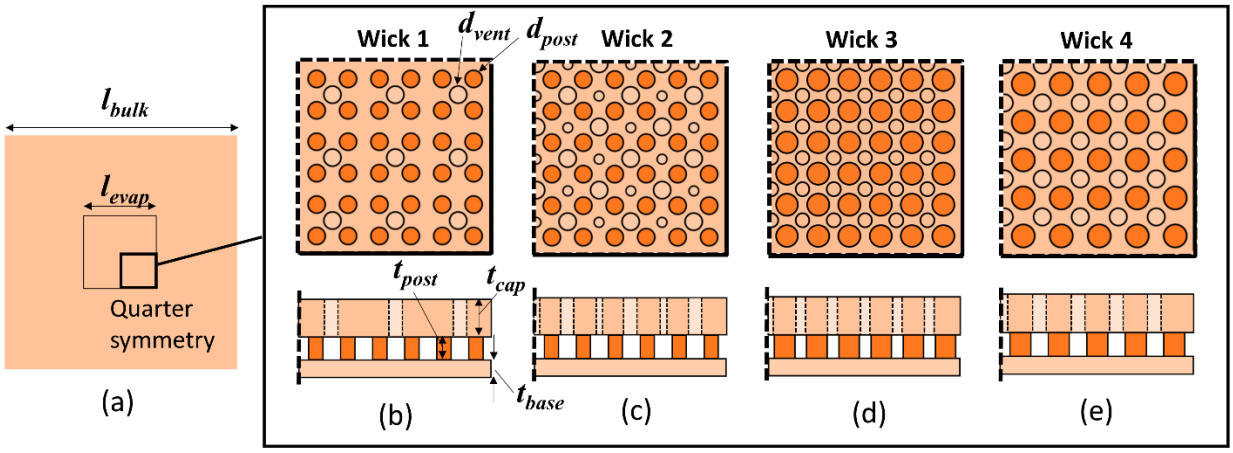

Figure 3. (a) Schematic diagram (top view) of the two-layer evaporator wick design; the square bulk wick region (side length l_{bulk} = 30 mm) supplies the square heated region (side length l_{evap} = 10 mm) where the two-layer wick features are fabricated. (b-e) Top-view and sectioned side-view schematic diagrams of Wicks 1-4. The top view diagrams are drawn to scale for one symmetric quadrant of the evaporator area; the open circles represent vents in the cap layer, while the filled circles represent the posts below. The side-view diagrams are not to scale in the thickness direction.

(note for editor: 2 columns wide)

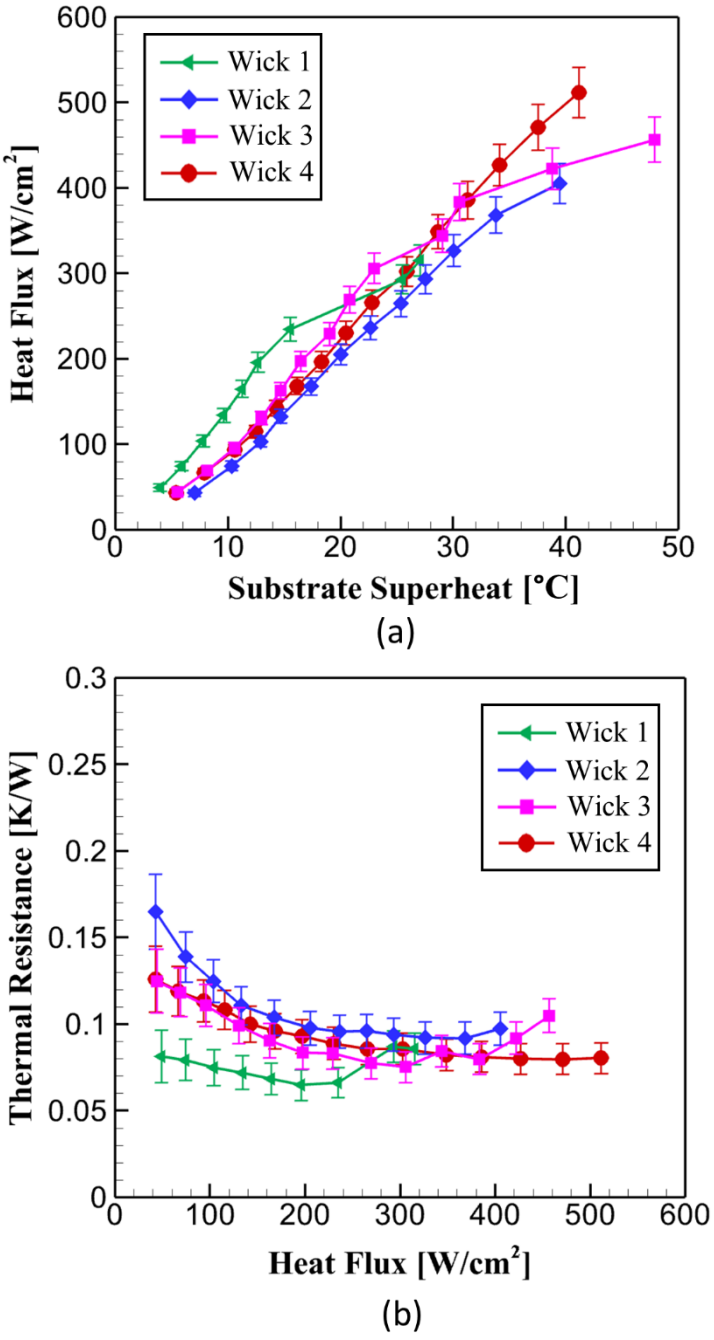

Figure 4. (a) Boiling curves and (b) wick thermal resistance curves for the four two-layer wick designs. The error bars in (a) and (b) represent the uncertainty in the heat flux and thermal resistance, respectively.

(note for editor: 1 column wide)

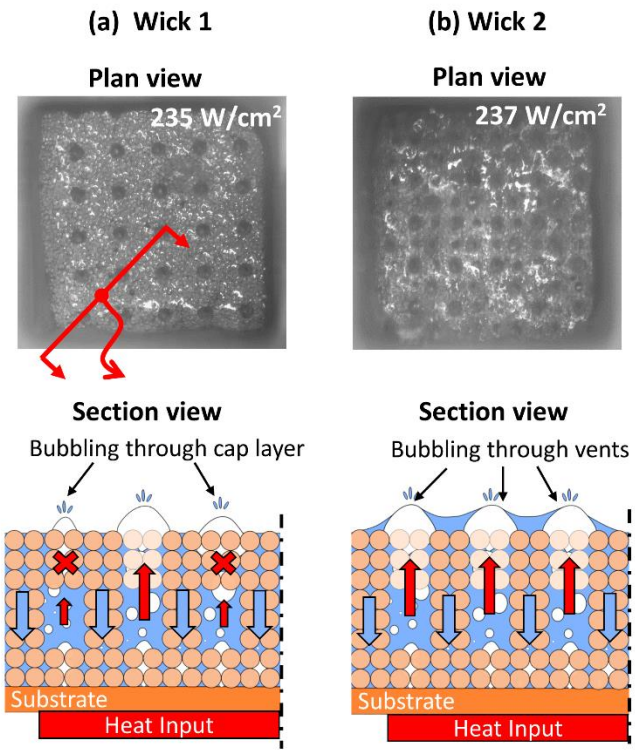

Figure 5. Plan-view images from high-speed visualization (see Appendix A for videos) taken during capillary-fed boiling in the two-layer wick, and section-view schematic diagrams depicting the observed boiling behavior, for (a) Wick 1 and (b) Wick 2 at similar heat flux of ~ 240 W/cm^2. Less vapor venting area for Wick 1 causes bubbling through the cap layer, which can disrupt liquid feeding to the substrate. Greater vapor venting area in Wick 2 ensures that vapor exits through the vents.

(note for editor: 1 column wide)

References

[1] A. Bar-Cohen, K. Matin, N. Jankowski, and D. Sharar, "Two-phase thermal ground planes: technology development and parametric results," *Journal of Electronics Packaging*, vol. 137, pp. 010801–9, 2014.

[2] J. A. Weibel and S. V. Garimella, "Recent advances in vapor chamber transport characterization for high-heat-flux applications," *Advances in Heat Transfer*, vol. 45, pp. 209–301, 2013.

[3] G. S. Hwang, E. Fleming, B. Carne, S. Sharratt, Y. Nam, P. Dussinger, Y. S. Ju and M. Kaviany, "Multi-artery heat-pipe spreader: Lateral liquid supply," *International Journal of Heat and Mass Transfer*, vol. 54, pp. 2334–2340, 2011.

[4] J. A. Weibel and S. V. Garimella, "Visualization of vapor formation regimes during capillary-fed boiling in sintered-powder heat pipe wicks," *International Journal of Heat and Mass Transfer* 55, pp. 3498–3510, 2012.

[5] T. Semenic, Y. Y. Lin, I. Catton, and D. B. Sarraf, "Use of biporous wicks to remove high heat fluxes," *Applied Thermal Engineering*, vol. 28, pp. 278–283, 2008.

[6] Q. Cai and Y.-C. Chen, "Investigations of biporous wick structure dryout," *Journal of Heat Transfer*, vol. 134, p. 021503, 2011.

[7] D. Ćoso, V. Srinivasan, M.-C. Lu, J.-Y. Chang, and A. Majumdar, "Enhanced heat transfer in biporous wicks in the thin liquid film evaporation and boiling regimes," *Journal of Heat Transfer*, vol. 134, p. 101501, 2012.

[8] Y. Nam, S. Sharratt, G. Cha, and Y. S. Ju, "Characterization and modeling of the heat transfer performance of nanostructured Cu micropost wicks," *Journal of Heat Transfer*, vol. 133, p. 101502, 2011.

[9] P. Xu and Q. Li, "Visualization study on the enhancement of heat transfer for the groove flat-plate heat pipe with nanoflower coated CuO layer," *Applied Physics Letters*, vol. 111, p. 141609, 2017.

[10] S. Sudhakar, J. A. Weibel, F. Zhou, E. M. Dede, and S. V. Garimella, "Area-scalable high-heat-flux dissipation at low thermal resistance using a capillary-fed two-layer evaporator wick," *International Journal of Heat and Mass Transfer*, vol. 135, pp. 1346–1356, 2019.

[11] F. Zhou, Y. Liu, and E. M. Dede, "Design, Fabrication, and Performance Evaluation of a Hybrid Wick Vapor Chamber," *Journal of Heat Transfer*, vol. 141, pp. 081802–8, 2019.

[12] X. Dai, F. Yang, R. Yang, Y.-C. Lee, and C. Li, "Micromembrane-enhanced capillary evaporation," *International Journal of Heat and Mass Transfer*, vol. 64, pp. 1101–1108, 2013.

[13] S. Ryu, J. Han, J. Kim, C. Lee, and Y. Nam, "Enhanced heat transfer using metal foam liquid supply layers for micro heat spreaders," *International Journal of Heat and Mass Transfer*, vol. 108, Part B, pp. 2338–2345, 2017.

[14] D. F. Hanks, Z. Lu, J. Sircar, T. R. Salamon, D. S. Antao, K. R. Bagnall, B. Barabadi and E. N. Wang, "Nanoporous membrane device for ultra high heat flux thermal management," *Microsystems & Nanoengineering*, vol. 4, 2018.

[15] S. Sudhakar, J. A. Weibel, and S. V. Garimella, "Design of an Area-Scalable Two-Layer Evaporator Wick for High-Heat-Flux Vapor Chambers," *IEEE Transactions on Components, Packaging and Manufacturing Technology*, vol. 9, pp. 458–472, 2019.

[16] S. Sudhakar, J. A. Weibel, and S. V. Garimella, "Experimental investigation of boiling regimes in a capillary-fed two-layer evaporator wick," *International Journal of Heat and Mass Transfer*, vol. 135, pp. 1335–1345, 2019.